The Extent and Rate of the Appearance of the Major 110 and 30 kDa Proteolytic Fragments during Post-Mortem Aging of Beef Depend on the Glycolysing Rate of the Muscle and Aging Time: An LC–MS/MS Approach to Decipher Their Proteome and Associated Pathways

Mohammed Gagaoua, Declan Troy, Anne Maria Mullen

The extent and rate of the appearance of the major 110 and 30 kDa proteolytic fragments during post-mortem aging of beef depend on the glycolysing rate of the muscle and aging time: an LC-MS/MS approach to decipher their proteome and associated pathways

Mohammed Gagaoua[1]*, Declan Troy[1], Anne Maria Mullen[1]

[1] Food Quality and Sensory Science Department, Teagasc Ashtown Food Research Centre, Ashtown, Dublin 15, Ireland

***Correspondence:** Dr. Mohammed Gagaoua

mohammed.gagaoua@teagasc.ie ; ORCID: 0000-0001-6913-3379

Abstract

Post-mortem (p-m) muscle undergoes a myriad of complex physical and biochemical changes, prior to its conversion to meat, which are influential on proteolysis and hence tenderisation. A more in-depth understanding of the mechanisms underpinning these dynamics is key to consistently providing tender beef. Using an LC-MS/MS approach, with state-of-art mass spectrometry Q Exactive HF-X, the proteome and associated pathways contributing to the appearance of the proteolytic breakdown products appearing over 14 days p-m, at two important molecular weights (110 and 30 kDa) on 1D SDS-PAGE gels, have been investigated in beef *Longissimus thoracis et lumborum* muscles exhibiting four rates of pH decline differentiated on the basis of time@pH6 (fast glycolysing < 3h; medium 3 -5 h; slow 5 – 8 h; and very slow 8+ h). Both 110 and 30 kDa bands appeared during aging and increased in intensity as a function of p-m time in a pH decline-dependent manner. The 110 kDa band appeared as early as 3h p-m and displayed an incremental increase in all groups through to 14 d p-m. From 2 d p-m, this increase in abundance during aging was significantly ($P < 0.001$) influenced by glycolytic rate: fast > or

= medium > slow > very slow. The day 2 p-m appearance of the 30 kDa band was most evident for fast glycolysing muscle with little or no evidence of appearance in slow and very slow. For day 7 and 14 p-m the strength of appearance was dependant on glycolysing groups*:* fast > medium > or = slow > very slow. LC-MS/MS analysis yielded a total of 22 unique proteins for the 110 kDa fragment and 13 for the 30 kDa, with 4 common proteins related to both actin and fibrinogen complex. The Gene Ontology analysis revealed a myriad of biological pathways are influential with many related to proteins involved primarily in muscle contraction and structure. Other pathways of interest include energy metabolism, apoptotic mitochondrial changes, calcium and ion transport, etc. Interestingly, most of the proteins composing the fragments were so far identified as biomarkers of beef tenderness and other quality traits.

Keywords: Beef tenderization; pH decline; Myofibrillar proteins; Metabolism; Proteomics

Introduction

Post-mortem (p-m) animal muscles undergo myriad and sophisticated physical and biochemical changes, which are responsible of their transformation into meat [1, 2]. These changes are first accompanied by a decrease in pH and temperature, described to be the former drivers of meat tenderization [3], hence affecting the osmotic pressure, the ionic strength of the muscle and the expressible juice[1, 2]. Furthermore, the extent of glycolysis and other energy metabolic pathways have a strong influence on many meat quality traits [4-6]. Their rate was considered to be a key determinant of tenderness through their impact on temperature and pH fall consequently orchestrating the activity of the endogenous muscle proteolytic enzymes [1, 7] and the apoptosis onset and development of *rigor mortis*[1, 8]. Many proteolytic systems such as calpains/calpastatin, cathepsins/cystatins, caspases/serpins, proteasomes and serine peptidases have been investigated *in vitro* for their impact on muscle degradation and beef tenderization [8-10]. Much of the research on p-m muscle protein changes has concentrated on the breakdown of the myofibrillar proteins with the main effects observed through fragmentation of proteins along the z-disc of the sarcomere [2, 11-13]. Therefore, a weakening and denaturation of muscle proteins and myofibrillar structure occur as a result of p-m storage of carcasses or meat cuts, which in turn leads to the tenderness experienced in cooked meat.

Recently and through the use of proteomics, muscle protein degradation has been further evidenced to be linked to energy metabolism (appearance of fragments of both glycolytic and oxidative enzymes including molecules from mitochondria), programmed cell death, heat shock proteins and oxidative stress among others [13-16]. However, inconsistencies in protein degradation occur and they are not fully understood. Among the studies that approached this aspect, some of them suggested that the underlying mechanisms are linked to the initial pH and extent of pH decline during the process of p-m glycolysis[17]. Others appointed the differences in the contractile and metabolic properties to variations in muscle fibres and their plasticity[6]. Recently,

and thanks to the use of liquid chromatography (LC) coupled to mass spectrometry (MS), Farouk's group from New Zealand highlighted that beef tenderization is likely to be compartmentalised by ultimate pH[18] when muscles were categorised as having low (≤ 5.79), medium (5.80 – 6.19) and high (≥ 6.2) ultimate pH. Further, the same group identified that depending on the ultimate pH category, different protein patterns and degradation rates of structural proteins can be observed [19]. However, the threshold level used of ultimate pH above 5.8 is considered by most beef companies, especially in Europe, to be of lower and more variable eating quality, hence leading to dark-cutting meat [20, 21]. Accordingly, in this study we targeted only carcasses that reached a pH of 5.8 or less in the loin muscle at the end of the maturation period (48 h p-m) and we considered for the first time four pH decline categories based on the time@pH6: fast < 3 h; medium 3 – 5 h; slow 5 – 8 h and very slow 8+ h. Hence, we hypothesized that the proteolysis extent will depend on the glycolysing rate of the p-m muscle. The identification of the proteome affected by the biochemical processes occurring during meat aging would contribute to deeper our understanding of the phenomenon of p-m beef aging. Therefore, this study aimed to decipher by means of LC-MS/MS and using the latest MS instrument in the benchtop Orbitrap series, the Q Exactive HF-X, the proteomic pathways involved in the appearance of two major proteolytic fragments running at two different molecular weights (low and high), whose intensities increased by increasing the aging time.

Materials and Methods

Animals, slaughtering and muscle sampling

Seventy eight crossbred beef cattle, representative of a typical commercial population, were slaughtered at an industrial meat plant (Dawn Meats group, Ballyhaunis, Republic of Ireland). From these, 12 heifers and 12 steers were selected to fit four pH decline rates as described below (n=3 per decline group for each gender). The animals were of similar age at slaughter (24 ± 1.9 months old) and carcass weight (325 ± 47 kg), and all finished to a specified fat cover

score (9.6 ± 1.4) and conformation (6.8 ± 2.1), both on a EUROP 1 – 15 scale. Slaughtering was performed in the morning under standardised conditions. Briefly, all animals were captive bolt stunned followed by exsanguination from the jugular vein and stun time was recorded as the point of reference for pH measurements. Then, the carcasses were dressed following the conventional commercial practices in compliance with the EU regulations (Council Regulation (EC) No. 1099/2009). Between 30 – 40 min post exsanguination, carcasses were split into two sides and then chilled at 10°C for 11 – 12 h, followed by storage in a 0°C chill until 48 h p-m. Samples of *Longissimus thoracis et lumborum* (LTL, mixed fast oxido-glycolytic) muscles were collected at four different p-m times (day 0 being 3h p-m, day 2 (48 h), day 7 and day 14). LTL muscle samples were removed, taking care to avoid connective tissue and subcutaneous or inter-muscular fat at 3hr p-m near the 4th lumbar from the right hand side of each carcass and immediately frozen in dry ice and transported to Teagasc, Ashtown for storage at -80°C. Second, striploin meat samples from the same carcasses side were taken on day 2 when they were quartered at the 5th rib. For this purpose, one steak of 2.5 cm thick close to the pH measurement point was cut into three parts (left, middle and right). The middle part was immediately used to take very carefully biopsies (day 2) free of fat and connective tissue. The two other parts were vacuum packaged and aged at 4°C for 7 (left) and 14 days (right) to sample the remaining biopsies. Storage of all the samples was performed at −80 °C until biochemical analyses.

pH measurement, modelling and kinetic data analysis

The pH of the LTL muscle was monitored by means of a portable pH meter (Orion Research Inc., Boston, USA) initially adjusted for muscle temperature and calibrated by two pH buffers being 4.0 and 7.0 before each set of measurements. pH was recorded at the 4th lumbar location at a depth of 4 cm at hourly intervals up to 8 h p-m and another measurement at 48 h p-m considered as the ultimate pH. From the experimental curves of pH decline p-m of each animal, an exponential equation with time p-m was used for fitting of the pH profile for rate constant

114 determination as a function of time using the parameterisation of an exponential decay
115 function[22]:

116 $$K = a - b\ x\ e^{(-c\ x\ t)}$$

117 where K represents the parameter,
118 a, its ultimate value,
119 b, the extent of its decline,
120 c, the rate of its decline,
121 and t, the time (h) p-m.

122 The variables a, b and c were calculated by minimizing the sum of squared residuals based on
123 the non-linear method of Newton Raphson algorithm [23]. The rate of pH decline was considered
124 in this study to characterize the animals in addition to the time @ pH 6.0 that allowed defining
125 four pH decline categories: fast < 3 h; medium 3 – 5 h; slow 5 – 8 h and very slow 8+ h.

126 ***Protein extractions and quantification***

127 Portions of the frozen muscle tissue samples from the four sampling times were used for
128 muscle proteins extractions. Briefly, 500 mg pieces of muscle were cut and weighed at – 20°C
129 to reduce artifactual protein degradation, subsequently incubated at 4°C for 10 min in 10 mL of
130 freshly prepared extraction buffer using Milli-Q purified water and containing 8 M urea, 2 M
131 thiourea, 1% DL-Dithiothreitol, 2% CHAPS, and 1.8% Pharmalyte® 3 - 10 (GE Healthcare,
132 Uppsala, Sweden). Next, the meat sample was homogenized for 40 sec (2 × 20 s with 20 s break
133 between bursts) using a T25 digital Ultra-Turrax® (IKA, Germany) at a high speed (15,000
134 rpm). The homogenates were incubated with shaking for 30 min on wet-ice, followed by a 30
135 min centrifugation at 10000 × g (Eppendorf 5424R, Eppendorf AG, Hamburg, Germany) and at
136 4°C to remove fat, insoluble proteins and any non-extracted cellular components. The pellet was
137 then solubilised in 5 mL of the same buffer and centrifuged under the same conditions for 10
138 min at 4°C. The supernatant was collected, fractionated and transferred into Eppendorf tubes
139 and stored at -80°C prior the proteomic analysis. Protein concentrations in triplicate were
140 determined using the Bio-Rad Protein Assay Kit (Bio-Rad Laboratories, Hercules, CA, USA)

based on the Bradford method. Bovine serum albumin (BSA) at a concentration of 1 mg/mL was used as standard. The extraction yield was the same within each sampling time for the four pH decline categories.

1D SDS-PAGE electrophoresis

Post-mortem proteolytic patterns were examined in 96 muscle protein extracts representing four sampling times (day 0, 2, 7 and 14) across the four pH decline categories (fast (F), medium (M), slow (S) and very slow (VS)) using one dimensional (1D) Sodium dodecyl sulphate – polyacrylamide gel electrophoresis (SDS-PAGE). This was carried out according to Laemmli [24] using 12% resolving and 4% stacking gels. Briefly, the protein extracts were first mixed at a ratio of 1.0:1.0 with sample buffer Laemmli 2× concentrate (#S3401, Sigma-Aldrich, St. Louis, USA) containing 4% w/v SDS, 20% v/v glycerol, 10% v/v β-mercaptoethanol, 125 mM Tris (pH 6.8) and 0.004% bromophenol blue, incubated at room temperature for 10 min and then heated (75°C) for 15 min in a standard block heater (VWR International). The denatured protein extracts in duplicate (20 µg per lane, 192 lanes in total) were then loaded and subjected to separate on a Mini-PROTEAN Tetra Cell system (Bio-Rad Laboratories, Hercules, CA, USA) for 3 h at 120 v using a TGS running buffer (#T7777, Sigma-Aldrich, Saint Louis, MO 63103, USA), which contains 25 mM Tris (pH 8.6), 192 mM glycine and 0.1% SDS. For each gel and in the first lane, 5 µL of a broad-range standard molecular weight marker (10–250 kDa, Precision Plus Protein™ Dual Color Standards, #161-0374, Bio-Rad Laboratories, Segrate-Milano, Italy) was included as a standard. Following completion of the separation, the gels were first washed twice in Milli-Q water for 5 min each time and stained overnight in 20 mL Coomassie Brilliant Blue G-250 based protein stain solution (EZBlue® gel staining reagent, Sigma-Aldrich, St. Louis, USA) with gentle shaking. The following morning, the gels were de-stained under shaking with Milli-Q water for 4h and washed twice before acquisition in transmission-scan mode by calibrated transparency densitometric scanner (GS-800, Bio-Rad)

using Bio-Rad Quantity One-4.5.2 software. Background subtraction was performed using the "lane background" function.

For band intensity quantification, all the protein bands in the scanned image gels (700 dpi and 16-bit) were quantified by Un-Scan-It gel 6.5 analysis program (Silk Scientific, Orem, UT) to estimate the molecular weights and optical intensities of the bands. The quantification of the band intensities aimed to identify the significant differences across pH decline group category and aging time. The data were exported to a Microsoft Excel spreadsheet and the densitometry of each band was normalized to the total density of the corresponding molecular weight in the entire row and expressed in arbitrary units (AU). Further, the data matrix was normalized per pH decline group and aging time. Then, a one-way ANOVA was used to detect the significant protein bands appearing as a consequence of proteolysis and differing with aging time across the four pH decline categories. Accordingly, two major and different proteolytic fragments were identified, these being the 30 and 110 kDa (**Figure 1**), which were considered of interest for LC-MS/MS identification and bioinformatics analyses.

LC–MS/MS analysis

The two proteolytic fragment bands appearing with an increase intensity during aging (at Day 2, 7 and 14) were excised by hand using sterile and disposable scalpels, de-stained, and prepared by reduction/alkylation, digestion by trypsin (Promega), peptide extraction, and drying [25] prior to LC-MS/MS using a Q Exactive HF-X hybrid quadrupole-Orbitrap mass spectrometer (Thermo Fisher Scientific). The hydrolysis of the bands was carried out with 48 µL of a 25mM ammonium bicarbonate buffer –12.5 ng/µL trypsin solution (Promega) per band for 5 h in an oven at 37 °C. A volume of 30 µL buffer was added periodically during hydrolysis so that the bands were always covered with liquid. The extraction of the peptides was carried out under ultrasonication for 15 min with 38.4 µl of 99.95% acetonitrile – 0.05 % trifluoroacetic acid. Then, the supernatant was transferred into 500 µL Eppendorf tubes and dry concentrated using a

Speedvac for 2 h. The volume was adjusted exactly to 20 µL with a solution of isotopologic peptides (50 pmol/µL) that is diluted 18 times in a 0.05 % TFA solution (internal quality control). After passing through the ultrasonic bath (10 min), the entire supernatant was transferred to an HPLC vial prior to LC-MS/MS analysis.

The separation step was carried out using a nano-HPLC Ultimate 3000 whereby, 2 µL of the protein hydolysate were first injected after pre-concentrated and desalted at a flow rate of 30 µL/min on a C18 pre-column 5 cm length × 100 µm (Acclaim PepMap 100 C18, 5µm, 100A nanoViper) equilibrated with Trifluoroacetic acid 0.05% in water to remove contaminants that could potentially disrupt the efficiency of the mass spectrometry analysis. After 6 min, the concentration column was switched online with a nanodebit analytical C18 column (Acclaim PepMap 100 - 75 µm inner diameter × 25 cm length; C18 - 3 µm -100Å - SN 10711310) operating at 400 nL/min equilibrated with 96 % solvent A (99.9 % H_2O, 0.1 % formic acid). The peptides were then separated according to their hydrophobicity, thanks to a gradient of solvent B, a solution of acetonitrile (ACN / FA-99.9 / 0.1) of 4 to 25% in 50 minutes. The nanoHPLC is coupled via a nanoESI source to an Orbitrap Q Exactive HFX mass spectrometer that operates in data dependent mode. The parent ion is selected in the orbitrap cell (FTMS) at a resolution of 60,000. Each MS analysis is succeeded by 18 MS/MS with analysis of the spectra fragments at a resolution of 15,000, microscan range of m/z 375 – 1600 and 60 s exclusion duration. The MS/MS spectra were analyzed using Proteome Discoverer V1.4.1 (ThermoFisher) and compared to *Bos taurus* Uniprot database (37,513 sequences, reference UP000009136_2020) using Mascot V 2.5 (http://www.matrixscience.com) with request parameters set: precursor mass tolerance to 10 ppm and fragment mass tolerance to 0.02 Da. For variable modifications, a maximum of two missed cleavages sites of trypsin was allowed including carbamidomethylation (C), methionine oxidation (M) and deamidation (NQ). Protein identification was validated when at least 2 unique peptides originating from one unique protein accession number showed statistically significant identity above Mascot scores of ≥ 28 with a False Discovery Rate (FDR)

of 1%. Furthermore, for the purpose of this study, we increased the confidence to a minimum of 4 unique peptides to accurately validate the proteins composing the 30 and 110 kDa proteolytic fragments.

Bioinformatics analyses

The LC-MS/MS yielded a total of 22 unique proteins for the 110 kDa fragment and 13 proteins for the 30 kDa (**Table 1** and **Table 2**), with 4 common proteins. The bovine UniprotIDs of the 31 proteins were converted[13] into the human orthologs EntrezGeneID to take advantage of the most complete annotation available. Therefore, both bovine and human UniprotIDs were indexed in the database and used. The process enrichment clustering was performed on Metascape® (https://metascape.org/) based on Kyoto Encyclopedia of Genes and Genomes (KEGG) pathways, Gene Ontology (GO) Biological Processes, and Reactome gene sets on the whole proteins as one dataset and for each proteolytic band fragment as separate datasets. Metascape® uses the hypergeometric test and Benjamini–Hochberg *p*-value correction algorithm to display the first statistically significant enriched ontology terms. In this study, the terms with a *P*-value < 0.05, a minimum count of 3, and an enrichment factor >1.5 (ratio between the observed counts and the counts expected by chance) were considered. Representative terms with a similarity score > 0.3 were clustered together based on their membership similarities and visualized in a network.

From the protein-protein interaction (PPI) network generated by Metascape®, the molecular complex detection (MCODE) algorithm was then used to detect densely connected regions (with default parameters) in the protein interaction network (neighbourhoods) if there are more than two proteins in a network. Pathway and process enrichment analysis were performed to each MCODE component independently and the significant scoring terms by p-value (Benjamini–Hochberg corrected) were retained as the functional description of the corresponding components. A unique colour was assigned to every MCODE network. A second PPI network

linking the 31 proteins from the 110 and 30 kDa polypeptides, including the molecular function was generated from the web-based search STRING database (https://string-db.org/). As an additional process, Metascape® was utilized to exhibit distribution of the 31 proteins among the two proteolytic fragments, based on a Circos plot which displays overlap and functional connections between the proteins. Subsequently, the known and potential targets based on the enriched terms among the two proteolytic fragments generated by the pathway and process enrichment analyses were compared and displayed by means of hierarchical heatmap clustering emphasizing the significant clusters.

Potential quantitative trait loci (QTL) were assessed using the ProteQTL tool included in ProteINSIDE (http://www.proteinside.org/) among the 31 proteins of the two proteolytic fragments appearing during aging. ProteQTL interrogates a public library of published QTL in Animal QTL Database (https://www.animalgenome.org/QTLdb) that contains cattle QTL and association data curated from published scientific articles. In this study, we considered three beef quality attributes available that are tenderness score, shear force and meat color lightness (L^*). Finally, a computational prediction of the putatively secreted proteins was performed on ProteINSIDE tool (http://www.proteinside.org/) identifying those potentially secreted through a signal peptide using the Signal P algorithm or by unconventional pathways of secretion (not involving a signal peptide) using the Target P algorithm.

Statistical analyses

The densitometry data of the protein fragments were analysed using the General Linear Model procedure of the SAS statistical software (SAS 9.3, SAS Institute INC, Cary, NC, USA). The test effects were pH decline group (fast, medium, slow and very slow) as the whole plot and aging time as the subplot (day 0, 2, 7 and 14). Gender effect was further considered included as random effect and no significant effect was observed and consequently removed. Least squares means were separated using Tukey test and considered significant if p-value is < 0.05. All

quantitative data were expressed as mean ± standard deviation (SD). A principal component analysis (PCA) of pH decline values was carried out using XLSTAT 2018.2 (AddinSoft, Paris, France) to highlight the separation of the pH decline groups.

Results

pH decline and protein changes over aging p-m time

Figure 1a shows the expected, clear separation of the four pH decline categories on the first two principal components. Individual variation is slightly higher for the fast glycolysing group (for which no overlap was observed with the other categories), compared to the other groups which are mostly grouped together, especially for the very slow glycolysing carcasses projected on the right. The divergence in the p-m pH decline curves among the four glycolysing groups was further confirmed by the significant differences ($P < 0.001$) in the pH decline rates (k values) computed for each glycolysing category (**Figure 1b**): 0.56 ± 0.08 pH unit/h for fast, 0.32 ± 0.04 pH unit/h for medium, 0.22 ± 0.02 pH unit/h for slow and 0.13 ± 0.03 pH unit/h for very slow group. **Figure 1c** shows a representative SDS-PAGE protein profile of the M. *longissimus thoracis et lumborum* muscle extracts at four different aging times sampled early p-m at day 0 (3h) and during aging at 2, 7 and 14 days p-m. The densitometry analysis on each gel (192 lanes in total) revealed the appearance of two major proteolytic fragment bands during p-m beef aging: 110 kDa (**Figure 1d**) and 30 kDa (**Figure 1e**). The relative abundance of the two protein fragments differ significantly ($P < 0.001$) within pH decline categories and across aging times with significant abundances by increasing the aging time period (**Table S1** and **Table S2**).

At day 0, only the 110 kDa fragment was appearing whatever the pH decline (in few animals only) with the highest abundance in medium glycolysing group and lowest in the very slow group (**Figure 1d**). At days 2 and 7 p-m, the abundance of this fragment was significantly ($P < 0.001$) higher for the fast and medium glycolysing rate carcasses compared to the slow and very slow (**Table S1**). At 14 days p-m a significant separation of the four curves is evident with

greater abundance for the fast group followed respectively by the medium, slow and very slow glycolysing categories. A stepwise increase in abundance from day 0 to day 14 was evident for all four pH decline categories. For the 30 kDa protein fragment, it first appeared at day 2 p-m (**Table S2**). Levels increased incrementally in all four groups from day 2 to day 14 p-m with the highest levels consistently observed in the fast glycolysing). At 2 days p-m, this fragment was mostly absent for the slow glycolysis (present in one carcass only) and not visible yet for any of the very slow carcasses (**Table S2**). The fragment was detectable in all the carcasses at 7 and 14 days p-m and as with the 110 kDa, greater abundances of the 30 kDa protein fragments were observed at both days for the fast glycolysing carcasses followed respectively by the medium, slow and very slow glycolysing categories (**Figure 1e**). The modelling of the relative abundances of the two protein fragments (**Figure 1f,g**) confirmed the trend of appearance described above, *i.e,* fastest for the fast glycolysing category, slower in medium and slow categories and slowest in the very slow glycolysing muscles, with significant separation of the curves within aging time and across the glycolysing rates. Further, the regression of the modelled protein bands abundances of the two fragments at 14 days p-m revealed that their appearance is concomitant with meat aging, especially for the fast group for which a high r-square > 0.98 was observed (**Figure 1h**). Finally, the findings of this trial indicated a greater degree of proteolysis in the fast glycolysing muscles in line with the earlier appearance of the 110 and 30 bands and the higher levels at day 14 p-m, which are indicative of more rapid proteolytic activity.

LC–MS/MS identification of the proteins composing the two major proteolytic fragments

To decipher the proteome content of the proteolytic fragments appearing at the 110 and 30 kDa zones during beef aging and the associated pathways, an LC-MS/MS approach provided identification of 22 unique proteins (with a minimum of 4 unique peptides) for the 110 kDa fragment (**Table 1**) and 13 proteins for the 30 kDa (**Table 2**). Four proteins, namely, ACTA1

317 (α-actin) and FGA, FGB and FGG (Fibrinogen α, β and ɣ chains, respectively) were common to
318 the two proteolytic fragments (**Figure 2a**).

319 The 22 proteins of the 110 kDa proteolytic fragment belong to five main biological pathways
320 (**Table 1**) from which half (n = 11) were (i) muscle contraction and structure proteins including
321 three myosin heavy chains isoforms (MYH1, MYH2 and MYH7), ACTA1, actinins (ACTN2
322 and ACTN3), nebulin (NEB), plectin (PLEC) and binding proteins (MYBPC1, MYBPC2 and
323 MYOM2). The (ii) catalytic and energy metabolism pathway grouped four enzymes: PYGM,
324 OGDH, PHKB and NNT (**Table 1**). These were followed by three (iii) fibrinogen complex
325 proteins FGA, FGB and FGG and (iv) proteolysis with two proteins: F2 which is a prothrombin
326 and PSMD1 which is a subunit of the 26S proteasome. The last pathway grouped two other
327 proteins (v) involved in calcium-binding and apoptotic mitochondrial changes, these being
328 ATP2A1 and SRL (**Table 1**). Thirteen of the 22 proteins are secreted proteins, from which 5 are
329 through a signal peptide (FGA, FGB, FGG, F2 and SRL) and 8 through pathways that do not
330 involve a signal peptide (ACTA1, ACTN2, ACTN3, NEB, PLEC, PYGM, PSMD1 and
331 ATP2A1).

332 The 13 proteins of the 30 kDa proteolytic fragment belong to four main biological pathways
333 (**Table 2**) with three pathways common to the 110 fragment. Three proteins were from the (i)
334 muscle contraction and structure, these being ACTA1, fast Troponin T (TNNT1) and MYL1
335 that is a myosin light chain. From (ii) the catalytic and energy metabolism pathway two
336 enzymes were identified: creatine kinase M-type (CKM) and mitochondrial 2-
337 oxoglutarate/malate carrier protein (SLC25A11). The third pathway grouped the three (iii)
338 fibrinogen complex proteins FGA, FGB and FGG (**Table 2**) followed by the last pathways,
339 which grouped five protein-binding, calcium and ion transport entities: B2M (beta-2-
340 microglobulin), VDAC3 (voltage-dependent anion-selective channel protein 3), PHB
341 (prohibitin), CA3 (carbonic anhydrase 3) and APOBEC2 (C->U-editing enzyme APOBEC-2).

Seven of the proteins of this fragment are secreted proteins from which four are through a signal peptide (FGA, FGB, FGG and B2M) and 3 through pathways that do not involve a signal peptide (ACTA1, VDAC3 and PHB).

Bioinformatics: functional enrichment analysis, clustering and protein-protein interaction

The process enrichment and cluster analysis pathways on the identified proteins based on GO and KEGG allowed the identification of 5 top and significant enriched terms (functional clusters) across the protein lists for the 110 kDa fragment (**Figure 2b**) and 3 for the 30 kDa (**Figure 2c**). The enrichment of the combined 31 proteins (two lists) highlighted in the order of importance (i) muscle filament sliding, (ii) fibrinogen complex and (iii) striated muscle contraction pathways as the top 3 enriched terms (**Figure 3d**). The heatmap comparing the protein lists and pathways between the two proteolytic fragments summarized the top 8 enriched term clusters (**Figure 3e**). The graph revealed that both muscle filament sliding (GO:0030049) and fibrinogen complex (CORUM:6417) are common to the two polypeptides (statistics details are given in **Table 3**), whereas anion transport term (GO:0006820) was specific to the 30 kDa fragment only and the terms skeletal muscle adaptation (GO:0043501), striated muscle contraction (GO:0006941), cell-substrate junction assembly (GO:0007044), energy derivation by oxidation of organic compounds (GO:0015980) and positive regulation of cation transmembrane transport (GO:1904064) were specific to the 110 kDa fragment (**Table 3** and **Figure 2e**). The association of these enriched terms and their functional enrichment was visualized by the network of **Figure 2f** showing once again the importance of muscle filament sliding and fibrinogen complex biological processes on beef aging. Furthermore, three significant sub-networks of high local network connectivity (MCODE 1–3) with 15 hub genes (proteins) were revealed from the PPI network based on MCODE analysis (**Figure 2g,h**). Of these, MCODE_1 evidencing the striated muscle contraction/filament sliding (ACTN2, ACTN3, MYBPC1, MYBPC2, NEB (110 kDa fragment), MYL1 and TNNT3 (30 kDa fragment)) had the

highest MCODE score (**Figure 2g**). MCODE_2 grouped FGA, FGB, FGG (for the two proteolytic fragments we targeted) and F2 (for 110 kDa fragment only) belonging to the fibrinogen complex and fibrinolysis pathway. MCODE_3 with the lowest MCODE score grouped 4 proteins that are OGDH, PYGM, PSMD1 (for 110 kDa fragment only) and VDAC3 (specific for the 30 kDa fragment) for the energy metabolism, anion transport and regulation pathway. The interconnectedness of these pathways was evidenced by the STRING network highlighting two major sub-networks (**Figure 3**), the striated muscle contraction/filament sliding (n = 12 proteins) and the fibrinogen complex and fibrinolysis (n = 4 proteins), that were both linked through the major components of the Z-line, alpha-actinin-2 (ACTN2).

Discussion

Tenderness is considered by consumers as a very important palatability trait driving the overall liking of cooked beef or influencing (re)purchasing decisions. However, inconsistency in the final eating quality has been identified as one of the major challenges facing the beef industry due to the wide range of factors impacting beef tenderness [26]. Among the post-slaughter and intrinsic factors, we hypothesised that variation in beef tenderness is related to differential response at the molecular/biochemical level within muscles during the early p-m carcass handling and aging periods. This trial has clearly demonstrated that during these periods and regardless of the pH decline rate, a myriad of biological pathways are being altered and these pathways relate to muscle contraction and structure, energy metabolism, apoptotic mitochondrial changes, calcium and ion transport, etc. In addition, we have demonstrated that these changes contribute to the appearance of two protein bands, which are newly created during the p-m period. While knowledge on these bands have increased over the past decades [2, 11, 17, 27, 28], this study is the first to decipher the proteome and associated pathways which are connected with the appearance of the 110 and 30 kDa bands. Further, this study confirmed previous

suggestions [7] that the rates of the appearance of these protein band fragments depend on the glycolysing rate of the muscle (pH decline category) as well as aging time.

Although since it was first proposed as a band of interest by Young, et al. [29], the 110 kDa has only been the focus of a handful of papers. Its importance was confirmed in the following decades [27] with the preliminary sequencing of this fragment taking place at the end of 90's by Troy, et al. [30]. The authors demonstrated an 80% homology with human C-protein for the first 17 amino acids sequenced. Our study has confirmed the presence of the C-protein, which is in fact the myosin-binding protein C represented in this study by two isoforms (MYBPC1, slow-type and MYBPC2, fast-type) in addition to 20 other proteins (**Table 1**). On the other hand, the 30 kDa band has been more extensively studied and was identified as an important marker of tenderization and a useful index to the progress of aging and proteolysis extent of muscle proteins degradation [2, 27, 28, 31-33]. The identity of this fragment was ascribed to originate from troponin T degradation [34, 35], but also proposed to contain actin fragments[1]. The LC-MS/MS used in this study enabled the identification of both troponin T (TNNT3) and actin (ACTA1) in keeping with the literature [1, 12, 16, 36]. However, we have also provided evidence that fragments from 11 other proteins are identifiable in this band (**Table 2**). Taken the above together, this study revealed using an appropriate *a priori* method (LC-MS/MS approach) that more than one protein composes the two protein proteolytic bands. These novel insights about such fragmentation products whose appearance are enhanced with aging and whose biological pathways are very important (for reviews: [1, 5, 13]), are potentially useful in more thoroughly understanding the processing underpinning beef tenderization. Interestingly, most of the proteins represented in these protein bands, as summarized in **Table 1** and **Table 2,** have also recently been identified in large integromics and proteomics studies[4, 13] to be biomarkers of beef tenderness (17 of 22 for the 110 kDa fragment and 9/13 for the 30 kDa) and colour traits (14/22 for the 110 kDa and 8/13 for the 30 kDa). Further, some of the proteins were reported to correlate with pH values and certain are drivers of pH decline (**Table 1** and **Table 2**). In the

following, we briefly present and discuss the main biological pathways which are represented in these two proteolytic protein bands appearing during p-m aging of beef *Longissimus thoracis* muscle.

Key role of the striated muscle contraction/filament sliding pathway during the p-m beef aging period

Almost half of the proteins (13 from 31) represented in both protein bands, but particularly the 110 kDa band, emanate from the muscle structure and contraction pathway. The predominance of this pathway adds further weight to the body of evidence linking the degree of the alteration and weakening of myofibrillar and cytoskeletal proteins during aging to the extent of proteolysis and meat tenderness development [5, 11, 13, 36, 37]. In fact, three interrelated GO terms grouped these proteins originating from the different parts of the sarcomere (**Table 3** and **Figure 2f**), with most of them also reported in a recent beef tenderness integromics meta-analysis [13]. Identification of proteins from the different parts of the sarcomere suggests that muscle structural breakdown occurs on the whole sarcomeric regions. Some of the identified proteins or their products can have MWs lower than the 110 kDa band. These are likely to be migrating in a cross-linked or aggregated form, a phenomenon that is reported previously [37]. Protein oxidation might further influence the protein solubility and the formation of aggregates. One other reason may be attributed to the existence of molecular complexes as proteins by their nature interact to form stoichiometrically stable complexes. This was confirmed here by the identification of a densely connected region of proteins (MCODE_1) from the striated muscle contraction/filament sliding pathway, which interacts with a second one (MCODE_2) via alpha-actinin-2 (ACTN2) (**Figure 3**) grouping the fibrinogen complex and fibrinolysis pathway (**Figure 2g,h**).

The action of endogenous muscle proteases on the myofibril structure can be postulated to be at the origin of the appearance of many of these new protein bands [8, 9, 12, 36]. Among the proteolytic systems, μ-calpain is the most investigated and known to be influenced by pH

442 decline [38], a fact which may have contributed to the more rapid p-m appearance of proteolysis
443 especially for the fast glycolysing carcasses in this study (**Figure 1f,g**). Indeed, a faster
444 glycolysis was reported to result in an early appearance of the autolyzed form of μ-calpain [38].
445 Caspases, the critical drivers of apoptosis, were also postulated to produce fragments early p-m
446 [39, 40] with MW of some proteins such as actin (ACTA1, identified in both bands in this study)
447 ranging from 14 to 32 kDa [1]. The role of cytoskeleton in apoptosis is well known and ACTA1 is
448 considered as a hallmark for apoptosis [1]. In addition, actin has been described as the first protein
449 targeted by executor caspases [1, 8], leading to a progressive upward trend of the appearance of the
450 major 30-32 kDa fragment, along with other lower MW fragments in p-m tissue[16, 36].
451 Proteasomes are further thought to play a role early p-m and some *in vitro* studies reported
452 activity in beef muscles up to one day [41] or 3 days [42]. On another hand, cathepsins B and L
453 activities during pre-rigor correlate positively with beef tenderness, especially in the fast
454 glycolysing muscles [7]. In agreement to our findings, an earlier study reported the appearance of
455 a band at 115 kDa from myosin heavy chain degradation following incubation of the muscle
456 with cathepsin L [43] which is like to equate to our 110 kDa band.

457 Identification of myosin superfamily members (MYH1, MYH2 and MYH7) in the 110 kDa
458 band agrees with the findings of Wu et al.[37] who focused on large proteins of beef muscle with
459 MW >100 kDa. Degradation of myosins, which are located in the thick filaments, and the
460 formation of new fragments at different MW have been demonstrated early p-m and during
461 aging [19, 36], exhibiting an important role in beef tenderness determination [13] as well as other
462 quality traits [4]. For example, myosin interacts with actin through the actin-myosin complex and
463 the myosin light chains, and if myosin, or the acto-myosin bond, is weakened during aging, the
464 tenderness of meat is affected [11, 12]. The identification of MYL1 (Myosin light chain 1/3) in the
465 30 kDa band is in line with the importance of this protein as a beef tenderness biomarker [13].
466 Myosin light chains are located near the heads of the myosins and the breakdown of the latter
467 may be at the origin of the appearance of the former.

The M-band and the Z-disk play also pivotal role in the assembly of the acto-myosin filament systems. Two proteins which are located in the M-band have been identified in this study: myomesin-2 (MYOM2) known also as M-protein [44] and CKM, the muscle isoform of creatine kinase that binds to central domains of both myomesin and M-protein [45]. During p-m aging, CKM is progressively fragmented [15, 16]. The rate of its fragmentation is associated with the rate of energy depletion and pH decline, explaining its identification in this trial and in large integromics studies as a robust biomarker of beef tenderness [13] and colour [4] and also as a QTL of colour lightness (**Table 4**).

Identification of MYOM2 in the 110 kDa band could be partly explained by their strong binding properties to myosins (**Figure 3**), which is in agreement with Wu et al.[37]. MYOM2 is a member of the immunoglobulin superfamily composed of immunoglobulin-like and fibronectin type III domains [44]. Several thick filament-associated proteins, also called myosin-binding proteins, belong to this immunoglobulin superfamily, such as myosin-binding protein C (MYBPC) anchored to the thick filament. MYBPC is a crucial component of the sarcomere and an important regulator of muscle function. For example, as well as binding myosin and actin [46] it also interacts with the giant actin-binding protein nebulin, identified in the 110 kDa band. Worthy to note that nebulin is highly prone to proteolysis by endogenous muscle proteases such as cathepsin L [9]. Since nebulin helps to link/anchor the thin filament firmly to the Z-disc, weakening of this link can trigger subsequent alterations in the myofibril during aging [47]. In this study, both isoforms of MYBPC formed a strong protein complex (MCODE_1) in the PPI network (**Figure 2g,h**). MYBPC1 was also a QTL of beef shear force (**Table 4**). Therefore we can postulate that MYBPC is of relevance when considering p-m aging of meat and in particular that it is influential in the rate of appearance of the 110 kDa fragment, and possibly that of the 30 kDa band, depending on the rate of pH decline (**Figure 1h**). As MYBPC might play a modulatory role in the regulation of actin-myosin interaction and by binding to both proteins it may directly affect calcium sensitivity. In fact, the earlier studies that searched the impact of

494 calcium and proteases inhibitors on myofibrils have shown that MYBPC can be solubilized by
495 calcium ions [48]. The solubilisation of this protein due to the influx of calcium into the muscle
496 cells may be then partly responsible of the weakening of the myofibrils and possibly increase
497 their susceptibility to proteolytic degradation. In support of this view, three proteins directly
498 involved in calcium homeostasis/flux were identified (**Table 1** and **Table 2**), these being
499 ATP2A1: sarcoplasmic/endoplasmic reticulum calcium ATPase 1 and SRL: sarcalumenin from
500 the 110 kDa band and a voltage-dependent anion channel (VDAC3), an abundant protein of the
501 outer mitochondrial membrane from the 30 kDa band. Calcium ions have also been involved in
502 the apoptosis onset through some signalling pathways [1]. As mentioned above, apoptosis affects
503 the integrity of the skeletal muscle by the means of the modification of calcium flux during
504 aging and its consequences on protein proteolysis involving ultra-structural changes [49].

505 The sarcomeric α-actinins (ACTN2 and ACTN3) are the other structural proteins identified
506 in the 110 kDa band (**Table 1**). They are actin-binding proteins that operate as major structural
507 components of the contractile apparatus at the Z-disc to stabilize the cytoskeleton, playing a role
508 in signalling and metabolic functions[50]. According to an earlier study, ACTN2 is the major
509 component present in all skeletal muscle fibres compared to ACTN3 which has more specialized
510 expression pattern and is expressed only in fast glycolytic skeletal muscle fibres[50]. In this trial,
511 ACTN3 was identified also as a QTL of tenderness score confirming its importance (**Table 4**).
512 However, it is ACTN2 that is essential for the integrity of the contractile apparatus through a
513 multitude of interactions (**Figure 2g,h**). For example, it is able to anchor certain cytoskeletal and
514 sarcomeric proteins including nebulin[51] and also to link the vascular extracellular matrix
515 glycoproteins and fibrinogen complex to myofibrils (**Figure 3**). Therefore, any degradation of
516 actinins by endogenous proteases or calcium flux would affect the structure of the sarcomere,
517 especially the Z-disc region. Finally, the other actin-binding, and giant protein, we identified in
518 the 110 kDa band, is plectin (PLEC) which is also known as an intermediate filament-based
519 versatile cytolinker protein. This is the only one of the parent proteins which has not, to date,

been identified as a beef tenderness biomarker. However, it was very recently reported as being of importance in the p-m aging of pork[52]. Further studies are warranted on plectin biochemistry in beef muscle to reveal potential roles in beef aging process and tenderization.

110 kDa and 30 kDa bands are influenced by pathways related to energy metabolism, mitochondria, apoptosis, calcium homeostasis and fibrinogen complex

The presence of sarcoplasmic fragments and products from other organelles, especially those related to mitochondria were very evident from our proteomic analysis. In this study, fragments from metabolic proteins and associated pathways were the second most abundant p-m changes identified to migrate within the two protein bands of interest. It is conceivable that p-m events in the muscle can lead to the presence of sarcoplasmic fractions and products from other organelles. These findings are in keeping with the current body of knowledge around tenderness determination and the aging process of meat[1, 5, 13, 14]. For example, proteomic-based studies on p-m protein degradation using protein fragments extracted from beef muscle during aging showed that among the enzymes we identified, creatine kinase (CKM, discussed previously) and glycogen phosphorylase (PYGM) are degraded [30, 53] and both were calpain substrates [54]. It is worth noting that PYGM, a rate-limiting enzyme of glycogenolysis, was identified on chromosome 29 as a QTL for both sensory tenderness and shear force (**Table 4**). The identification of glycogen phosphorylase kinase β-subunit (PHKB), a regulatory enzyme of glycogen metabolism, in the 110 kDa band is consistent with the presence of PYGM. Calcium is the main regulator of PHKB[55] further supporting the identification of major proteins in the same band that play roles in calcium homeostasis (ATP2A1 and SRL presented above). Moreover, both PYGM and PHKB were related to pH decline (**Table 1**). OGDH (2-oxoglutarate dehydrogenase) and NNT (NAD(P) transhydrogenase) from the 110 kDa band and SLC25A11 (Mitochondrial 2-oxoglutarate/malate carrier protein) from the 30 kDa band are metabolic enzymes related to mitochondria (**Table 1** and **Table 2**). The three enzymes were previously

545 identified as biomarkers of beef tenderness[13], hence pointing their importance in beef aging.
546 OGDH catalyses the conversion of α- ketoglutarate to succinyl coenzyme A, a critical step in the
547 Krebs cycle, while SLC25A11 and NNT have multiple functions. NNT is involved in the
548 detoxification of reactive oxygen species and regulation of isocitrate dehydrogenase activity.
549 SLC25A11 catalyzes the transport of 2-oxoglutarate across the inner mitochondrial membrane
550 in an electroneutral exchange for malate or other dicarboxylic acids, and plays an important role
551 in several metabolic processes, including the malate-aspartate shuttle, the oxoglutarate/isocitrate
552 shuttle, and gluconeogenesis from lactate[56]. In addition, SLC25A11 maintains mitochondrial
553 fusion and fission events proposed to play a role in the conversion of muscle into meat[1], as well
554 as in the regulation of apoptosis. Other proteins from the 30 kDa fragment, these being PHB
555 (Prohibitin), CA3 (Carbonic anhydrase 3) and APOBEC2 (C->U-editing enzyme APOBEC-2)
556 were all identified as biomarkers of beef tenderness[13]. Among them, prohibitin plays several
557 roles especially in the morphogenesis of mitochondrial cristae including the mitochondrial
558 fusion and fission events[57]. CA3 is a marker of cell detoxification [1], known to be involved in the
559 regulation of the cellular pH in the living cell[58]. We suggest that CA3 would play a role in the
560 differences observed in the rates of pH decline among the four glycolysing groups of this trial.

561 Finally, we have revealed for the first time the presence in both bands of peptides related to
562 the fibrinogen complex with its three protein isoforms: FGA, FGB and FGG for fibrinogen α, β
563 and ɣ chains, respectively (**Table 1** and **Table 2**). Fibrinogen is known as extracellular matrix
564 (ECM) glycoproteins and categorized as vascular ECM proteins[59]. Fibrinogen, is a soluble
565 macromolecule, but forms a clot or insoluble gel on conversion to fibrin by the action of the
566 serine proteolytic enzyme thrombin[60]. We suppose that it is through prothrombin (F2) identified
567 in the 110 kDa fragment that fibrinogen was identified to be related to the tenderizing process of
568 meat. Also, fibrinogen has both strong and weak binding sites for calcium ions, which are
569 important for its structural stability and functions[60]. In its various functions as a clotting and
570 adhesive protein, the fibrinogen molecule is involved in many intermolecular interactions and

has specific binding sites for several proteins as shown in **Figure 2f** and **Figure 3**. In the context of muscle to meat conversion, fibrinogen is not well studied. Thus, further investigations are warranted to understand if it is a causative factor in p-m aging or if it is indicative of other processes happening during this period *e.g.* aggregation, proteolysis etc.

To conclude, this study has revealed the first detailed map of several interconnected pathways which are involved in the concomitant appearance of the 110 and 30 kDa SDS-PAGE bands as two major proteolytic fragments among others appearing during aging/tenderizing process of beef *Longissimus thoracis et lumborum* muscles. Interestingly, we have provided strong evidence that the appearance of the fragments is pH decline dependent, being most prevalent in fast glycolysing carcasses. This in-depth proteome analysis of the two protein bands has revealed that most of the identified parent proteins have been identified as biomarkers of beef tenderness and other quality traits, thus providing further clarity on the intricacies of these relationships in light of p-m glycolytic rates. .

Declaration of competing interest

The authors declared that there is no conflict of interest.

Acknowledgements

Dr. Mohammed Gagaoua is a Marie Skłodowska-Curie Career-FIT Fellow under the number MF20180029. He is grateful to the funding received from the Marie Skłodowska-Curie grant agreement No. 713654 and the support of Meat Technology Ireland a co-funded industry/Enterprise Ireland project (TC 2016 002). We convey special thanks to Mr. Peter Mooney from Innovation@Dawn at Dawn Meats Group for his great support and collaboration. We gratefully thank Mr. Didier Viala from the Metabolomic and Proteomic Exploration Facility (PFEM), INRAE Auvergne-Rhône-Alpes, France for the mass spectrometry analyses. The authors acknowledge the support and technical help of Dr. John Colreavy, Dr. Cormac k. McElhinney and Dr. Michael Whelan from Meat Technology Ireland; Mr. Dan Galvin, Mr. Joe

Calvey and Mss. Shauna Morley from Dawn Meats Group; and Dr. Ruth Hamill, Dr. Carlos Alvarez, Mr. Eugene Vesey and Mr. Yao Zhu from Teagasc, Ashtown.

References

1. Ouali, A.; Gagaoua, M.; Boudida, Y.; Becila, S.; Boudjellal, A.; Herrera-Mendez, C. H.; Sentandreu, M. A., Biomarkers of meat tenderness: present knowledge and perspectives in regards to our current understanding of the mechanisms involved. *Meat science* **2013**, *95*, 854-70.

2. Ouali, A., Meat Tenderization: Possible Causes and Mechanisms. A Review. *Journal of Muscle Foods* **1990**, *1*, 129-165.

3. Koohmaraie, M.; Geesink, G. H., Contribution of postmortem muscle biochemistry to the delivery of consistent meat quality with particular focus on the calpain system. *Meat science* **2006**, *74*, 34-43.

4. Gagaoua, M.; Hughes, J.; Terlouw, E. M. C.; Warner, R. D.; Purslow, P. P.; Lorenzo, J. M.; Picard, B., Proteomic biomarkers of beef colour. *Trends in Food Science & Technology* **2020**, *101*, 234-252.

5. Picard, B.; Gagaoua, M., Meta-proteomics for the discovery of protein biomarkers of beef tenderness: An overview of integrated studies. *Food Res Int* **2020**, *127*, 108739.

6. Picard, B.; Gagaoua, M., Muscle Fiber Properties in Cattle and Their Relationships with Meat Qualities: An Overview. *J Agric Food Chem* **2020**, *68*, 6021-6039.

7. O'Halloran, G. R.; Troy, D. J.; Buckley, D. J.; Reville, W. J., The role of endogenous proteases in the tenderisation of fast glycolysing muscle. *Meat science* **1997**, *47*, 187-210.

8. Kemp, C. M.; Sensky, P. L.; Bardsley, R. G.; Buttery, P. J.; Parr, T., Tenderness--an enzymatic view. *Meat science* **2010**, *84*, 248-56.

9. Sentandreu, M. A.; Coulis, G.; Ouali, A., Role of muscle endopeptidases and their inhibitors in meat tenderness. *Trends in Food Science & Technology* **2002**, *13*, 400-421.

10. Gagaoua, M.; Hafid, K.; Boudida, Y.; Becila, S.; Ouali, A.; Picard, B.; Boudjellal, A.; Sentandreu, M. A., Caspases and Thrombin Activity Regulation by Specific Serpin Inhibitors in Bovine Skeletal Muscle. *Appl Biochem Biotechnol* **2015**, *177*, 279-303.

11. Taylor, R. G.; Geesink, G. H.; Thompson, V. F.; Koohmaraie, M.; Goll, D. E., Is Z-disk degradation responsible for postmortem tenderization? *Journal of Animal Science* **1995**, *73*, 1351-1367.

12. Huff-Lonergan, E.; Zhang, W.; Lonergan, S. M., Biochemistry of postmortem muscle - lessons on mechanisms of meat tenderization. *Meat science* **2010**, *86*, 184-95.

13. Gagaoua, M.; Terlouw, E. M. C.; Mullen, A. M.; Franco, D.; Warner, R. D.; Lorenzo, J. M.; Purslow, P. P.; Gerrard, D.; Hopkins, D. L.; Troy, D.; Picard, B., Molecular signatures of beef tenderness: Underlying mechanisms based on integromics of protein biomarkers from multi-platform proteomics studies. *Meat science* **2021**, *172*, 108311.

14. Picard, B.; Gagaoua, M., Chapter 11 - Proteomic Investigations of Beef Tenderness. In *Proteomics in Food Science: from farm to fork*, Colgrave, M. L., Ed. Academic Press: London, 2017; pp 177-197.

15. Jia, X.; Hildrum, K. I.; Westad, F.; Kummen, E.; Aass, L.; Hollung, K., Changes in enzymes associated with energy metabolism during the early post mortem period in longissimus thoracis bovine muscle analyzed by proteomics. *J Proteome Res* **2006**, *5*, 1763-9.

16. Laville, E.; Sayd, T.; Morzel, M.; Blinet, S.; Chambon, C.; Lepetit, J.; Renand, G.; Hocquette, J. F., Proteome changes during meat aging in tough and tender beef suggest the importance of apoptosis and protein solubility for beef aging and tenderization. *J Agric Food Chem* **2009**, *57*, 10755-64.

17. White, A.; O'Sullivan, A.; Troy, D. J.; O'Neill, E. E., Manipulation of the pre-rigor glycolytic behaviour of bovine M. longissimus dorsi in order to identify causes of inconsistencies in tenderness. *Meat science* **2006**, *73*, 151-156.

18. Lomiwes, D.; Farouk, M. M.; Wu, G.; Young, O. A., The development of meat tenderness is likely to be compartmentalised by ultimate pH. *Meat science* **2014**, *96*, 646-651.

19. Wu, G.; Farouk, M. M.; Clerens, S.; Rosenvold, K., Effect of beef ultimate pH and large structural protein changes with aging on meat tenderness. *Meat science* **2014**, *98*, 637-45.

20. Gagaoua, M.; Picard, B.; Monteils, V., Associations among animal, carcass, muscle characteristics, and fresh meat color traits in Charolais cattle. *Meat science* **2018**, *140*, 145-156.

21. Ponnampalam, E. N.; Hopkins, D. L.; Bruce, H.; Li, D.; Baldi, G.; Bekhit, A. E.-d., Causes and Contributing Factors to "Dark Cutting" Meat: Current Trends and Future Directions: A Review. *Comprehensive Reviews in Food Science and Food Safety* **2017**, *16*, 400-430.

22. Hwang, I. H.; Thompson, J. M., The interaction between pH and temperature decline early postmortem on the calpain system and objective tenderness in electrically stimulated beef longissimus dorsi muscle. *Meat science* **2001**, *58*, 167-174.

23. Zamora, F.; Aubry, L.; Sayd, T.; Lepetit, J.; Lebert, A.; Sentandreu, M. A.; Ouali, A., Serine peptidase inhibitors, the best predictor of beef ageing amongst a large set of quantitative variables. *Meat science* **2005**, *71*, 730-42.

24. Laemmli, U. K., Cleavage of structural proteins during the assembly of the head of bacteriophage T4. *Nature* **1970**, *227*, 680-5.

25. Picard, B.; Kammoun, M.; Gagaoua, M.; Barboiron, C.; Meunier, B.; Chambon, C.; Cassar-Malek, I., Calcium Homeostasis and Muscle Energy Metabolism Are Modified in HspB1-Null Mice. *Proteomes* **2016**, *4*, 17.

26. Gagaoua, M.; Picard, B.; Monteils, V., Assessment of cattle inter-individual cluster variability: the potential of continuum data from the farm-to-fork for ultimate beef tenderness management. *J Sci Food Agric* **2019**, *99*, 4129-4141.

27. Koohmaraie, M.; Kennick, W. H.; Elgasim, E. A.; Anglemier, A. F., Effects of Postmortem Storage on Muscle Protein Degradation: Analysis by SDS-Polyacrylamide Gel Electrophoresis. *Journal of Food Science* **1984**, *49*, 292-293.

28. Olson, D. G.; Parrish, F. C., Relationship of Myofibril Fragmentation Index to Measures of Beefsteak Tenderness. *Journal of Food Science* **1977**, *42*, 506-509.

29. Young, O. A.; Graafhuis, A. E.; Davey, C. L., Post-mortem changes in cytoskeletal proteins of muscle. *Meat science* **1980**, *5*, 41-55.

30. Troy, D.; Patyaryas, T.; Tsitsilonis, R.; Yialouris, P.; Vazeou, V.; Healy, A.; Stoeva, S.; Voelter, W. In *Sequence analysis of proteins extracted from bovine myofibrillar extracts during the ageing*

period, ANNUAL INTERNATIONAL CONGRESS OF MEAT SCIENCE AND TECHNOLOGY, 1997; 1997; pp 698-699.

31. Macbride, M. A.; Parrish, F. C., The 30,000-Dalton Component of Tender Bovine Longissimus Muscle. *Journal of Food Science* **1977**, *42*, 1627-1629.

32. Kołczak, T.; Pospiech, E.; Palka, K.; Łącki, J., Changes of myofibrillar and centrifugal drip proteins and shear force of psoas major and minor and semitendinosus muscles from calves, heifers and cows during post-mortem ageing. *Meat science* **2003**, *64*, 69-75.

33. Penny, I. F.; Ferguson-Pryce, R., Measurement of autolysis in beef muscle homogenates. *Meat science* **1979**, *3*, 121-134.

34. Ho, C. Y.; Stromer, M. H.; Robson, R. M., Identification of the 30 kDa polypeptide in post mortem skeletal muscle as a degradation product of troponin-T. *Biochimie* **1994**, *76*, 369-375.

35. Negishi, H.; Yamamoto, E.; Kuwata, T., The origin of the 30 kDa component appearing during post-mortem ageing of bovine muscle. *Meat science* **1996**, *42*, 289-303.

36. Lana, A.; Zolla, L., Proteolysis in meat tenderization from the point of view of each single protein: A proteomic perspective. *Journal of Proteomics* **2016**, *147*, 85-97.

37. Wu, G.; Clerens, S.; Farouk, M. M., LC MS/MS identification of large structural proteins from bull muscle and their degradation products during post mortem storage. *Food Chem* **2014**, *150*, 137-44.

38. Pomponio, L.; Ertbjerg, P.; Karlsson, A. H.; Costa, L. N.; Lametsch, R., Influence of early pH decline on calpain activity in porcine muscle. *Meat science* **2010**, *85*, 110-114.

39. Huang, F.; Huang, M.; Zhou, G.; Xu, X.; Xue, M., In Vitro Proteolysis of Myofibrillar Proteins from Beef Skeletal Muscle by Caspase-3 and Caspase-6. *Journal of Agricultural and Food Chemistry* **2011**, *59*, 9658-9663.

40. Kemp, C. M.; Bardsley, R. G.; Parr, T., Changes in caspase activity during the postmortem conditioning period and its relationship to shear force in porcine longissimus muscle. *J Anim Sci* **2006**, *84*, 2841-6.

41. Robert, N.; Briand, M.; Taylor, R.; Briand, Y., The effect of proteasome on myofibrillar structures in bovine skeletal muscle. *Meat science* **1999**, *51*, 149-153.

42. Dutaud, D.; Aubry, L.; Guignot, F.; Vignon, X.; Monin, G.; Ouali, A., Bovine muscle 20S proteasome. II: Contribution of the 20S proteasome to meat tenderization as revealed by an ultrastructural approach. *Meat science* **2006**, *74*, 337-344.

43. Mikami, M.; Whiting, A. H.; Taylor, M. A. J.; Maciewicz, R. A.; Etherington, D. J., Degradation of myofibrils from rabbit, chicken and beef by cathepsin l and lysosomal lysates. *Meat science* **1987**, *21*, 81-97.

44. Lange, S.; Pinotsis, N.; Agarkova, I.; Ehler, E., The M-band: The underestimated part of the sarcomere. *Biochimica et Biophysica Acta (BBA) - Molecular Cell Research* **2020**, *1867*, 118440.

45. Hornemann, T.; Kempa, S.; Himmel, M.; Hayeß, K.; Fürst, D. O.; Wallimann, T., Muscle-type Creatine Kinase Interacts with Central Domains of the M-band Proteins Myomesin and M-protein. *Journal of Molecular Biology* **2003**, *332*, 877-887.

46. Ackermann, M. A.; Kontrogianni-Konstantopoulos, A., Myosin Binding Protein-C: A Regulator of Actomyosin Interaction in Striated Muscle. *Journal of Biomedicine and Biotechnology* **2011**, *2011*, 636403.

716 47. Fritz, J. D.; Greaser, M. L., Changes in Titin and Nebulin in Postmortem Bovine Muscle
717 Revealed by Gel Electrophoresis, Western Blotting and Immunofluorescence Microscopy. *Journal of*
718 *Food Science* **1991**, *56*, 607-610.

719 48. Taylor, M. A. J.; Etherington, D. J., The solubilization of myofibrillar proteins by calcium ions.
720 *Meat science* **1991**, *29*, 211-219.

721 49. Pinton, P.; Giorgi, C.; Siviero, R.; Zecchini, E.; Rizzuto, R., Calcium and apoptosis: ER-
722 mitochondria Ca2+ transfer in the control of apoptosis. *Oncogene* **2008**, *27*, 6407-6418.

723 50. Lek, M.; Quinlan, K. G. R.; North, K. N., The evolution of skeletal muscle performance: gene
724 duplication and divergence of human sarcomeric α-actinins. *BioEssays* **2010**, *32*, 17-25.

725 51. Nave, R.; Fürst, D. O.; Weber, K., Interaction of α-actinin and nebulin in vitro. *FEBS Letters*
726 **1990**, *269*, 163-166.

727 52. Tian, X.; Wang, Y.; Fan, X.; Shi, Y.; Zhang, W.; Hou, Q.; Liu, R.; Zhou, G., Expression of Pork
728 Plectin during Postmortem Aging. *Journal of Agricultural and Food Chemistry* **2019**, *67*, 11718-11727.

729 53. Stoeva, S.; Byrne, C. E.; Mullen, A. M.; Troy, D. J.; Voelter, W., Isolation and identification of
730 proteolytic fragments from TCA soluble extracts of bovine M. longissimus dorsi. *Food Chemistry* **2000**,
731 *69*, 365-370.

732 54. Purintrapiban, J.; Wang, M.-c.; Forsberg, N. E., Identification of glycogen phosphorylase and
733 creatine kinase as calpain substrates in skeletal muscle. *The International Journal of Biochemistry & Cell*
734 *Biology* **2001**, *33*, 531-540.

735 55. Brostrom, C. O.; Hunkeler, F. L.; Krebs, E. G., The regulation of skeletal muscle phosphorylase
736 kinase by Ca2+. *The Journal of biological chemistry* **1971**, *246*, 1961-7.

737 56. Pan, G.; Wang, R.; Jia, S.; Li, Y.; Jiao, Y.; Liu, N., SLC25A11 serves as a novel prognostic
738 biomarker in liver cancer. *Scientific Reports* **2020**, *10*, 9871.

739 57. Merkwirth, C.; Langer, T., Prohibitin function within mitochondria: Essential roles for cell
740 proliferation and cristae morphogenesis. *Biochimica et Biophysica Acta (BBA) - Molecular Cell*
741 *Research* **2009**, *1793*, 27-32.

742 58. Duda, D. M.; Tu, C.; Fisher, S. Z.; An, H.; Yoshioka, C.; Govindasamy, L.; Laipis, P. J.;
743 Agbandje-McKenna, M.; Silverman, D. N.; McKenna, R., Human Carbonic Anhydrase III: Structural
744 and Kinetic Study of Catalysis and Proton Transfer. *Biochemistry* **2005**, *44*, 10046-10053.

745 59. Hynes, R. O.; Naba, A., Overview of the Matrisome—An Inventory of Extracellular Matrix
746 Constituents and Functions. *Cold Spring Harbor Perspectives in Biology* **2012**, *4*.

747 60. Weisel, J. W., Fibrinogen and Fibrin. In *Advances in Protein Chemistry*, Academic Press: 2005;
748 Vol. 70, pp 247-299.

749

Figure captions

Figure 1. pH decline and protein changes over p-m aging time. **a)** Scores plot of the separation of the individuals (n = 6 per group) characterizing the four pH decline categories (with different glycolysing rate): fast (F, ●), medium (M, ♦), slow (S, ▲) and very slow (VS, ■) using principal component analysis. The loadings were based on pH values measured on carcass (10°C chill) at the 4th lumbar from 1hr to 8hr p-m. **b)** Variance analysis comparing the calculated pH decline rates (*k*) for each category at a significant level of 5%. **c)** Representative 1D SDS–PAGE profile of Colloid Coomassie-stained (EZBlue® gel staining reagent) 12% polyacrylamide gel of beef *M. longissimus thoracis et lumborum* muscle extracts at four different aging times starting from day 0 (biopsy samples taken at 3hr p-m). The first lane corresponds to the molecular weights (Mw) standards in kiloDaltons (kDa). **d, e)** Densitometry analyses of the 110 and 30 kDa protein band fragments appearing during p-m aging time as a function of pH decline (glycolysing rate) and aging time (**Table S1** and **Table S2** for details of the variance analyses). The quantity changes of the proteins were expressed in arbitrary units (means ± standard deviation). **f**, **g)** Exponential curves representing formation of the 110 kDa and 30 kDa protein fragments over aging time. The average estimate slopes of the curves are given for each pH decline category. **h)** Linear regression between the protein quantities at day 14 p-m (D14) of the 110 kDa and 30 kDa protein fragments.

Figure 2. Biological pathways and process enrichment cluster analysis using Metascape® (https://metascape.org/) on the 31 proteins identified from the two proteolytic 110 kDa and 30 kDa band fragments. **a)** Circos plot showing the common 4 proteins between the 110 kDa and 30 kDa proteolytic fragments. **b–d)** GO and KEGG analyses of the **b)** 22 proteins from the 110 kDa fragment, **c)** 13 proteins from the 30 kDa fragment, and **d)** total 31 proteins from both fragments. The bar graphs highlight the top enriched terms (functional clusters) across the protein lists coloured according to *P*-values: terms with a *P*-value < 0.01, a minimum count of 3, and an enrichment factor > 1.5. **e)** Heatmap based on the protein lists between the two proteolytic fragments showing the top 8 enriched term clusters, one row per cluster, using a discrete colour scale by *P*-values to represent statistical significance. Grey indicates a lack of significance. **f)** Enrichment network visualization for results from the proteins present in each of the 8 clusters identified coloured by cluster ID (details in **Table 3**), where nodes that share the same cluster ID are typically close to each other. In the term networks, nodes are coloured by term, where terms with a similarity >0.3 are connected by edges. **g)** Key most significant molecular complex detection (MCODE) components form the network. Each node represents a protein, and the edge between nodes represents the interaction between two connected proteins. **h)** The same MCODE

783 components (modules) by highlighting to which proteolytic fragment the proteins belong.
784 Abbreviations: GO *gene ontology*, KEGG *Kyoto Encyclopedia of Genes and Genomes pathways*.

785 **Figure 3.** Protein-protein interaction (PPI) network linking the whole 31 proteins from the 110 and
786 30 kDa proteolytic protein band fragments, highlighting also the molecular function. The
787 interaction map was generated from the web-based search STRING database (https://string-
788 db.org/). Network statistics are: number of nodes: 31; number of edges: 114; average node degree:
789 7.35; average local clustering coefficient: 0.735; expected number of edges: 9 and PPI enrichment
790 *p*-value: $< 1.0e^{-16}$. The secreted proteins among the 31 proteins were further shown by small
791 yellow ovals on each protein for those secreted using a signal peptide (conventional pathway) and
792 by orange ovals for those pathways that do not involve a signal peptide.

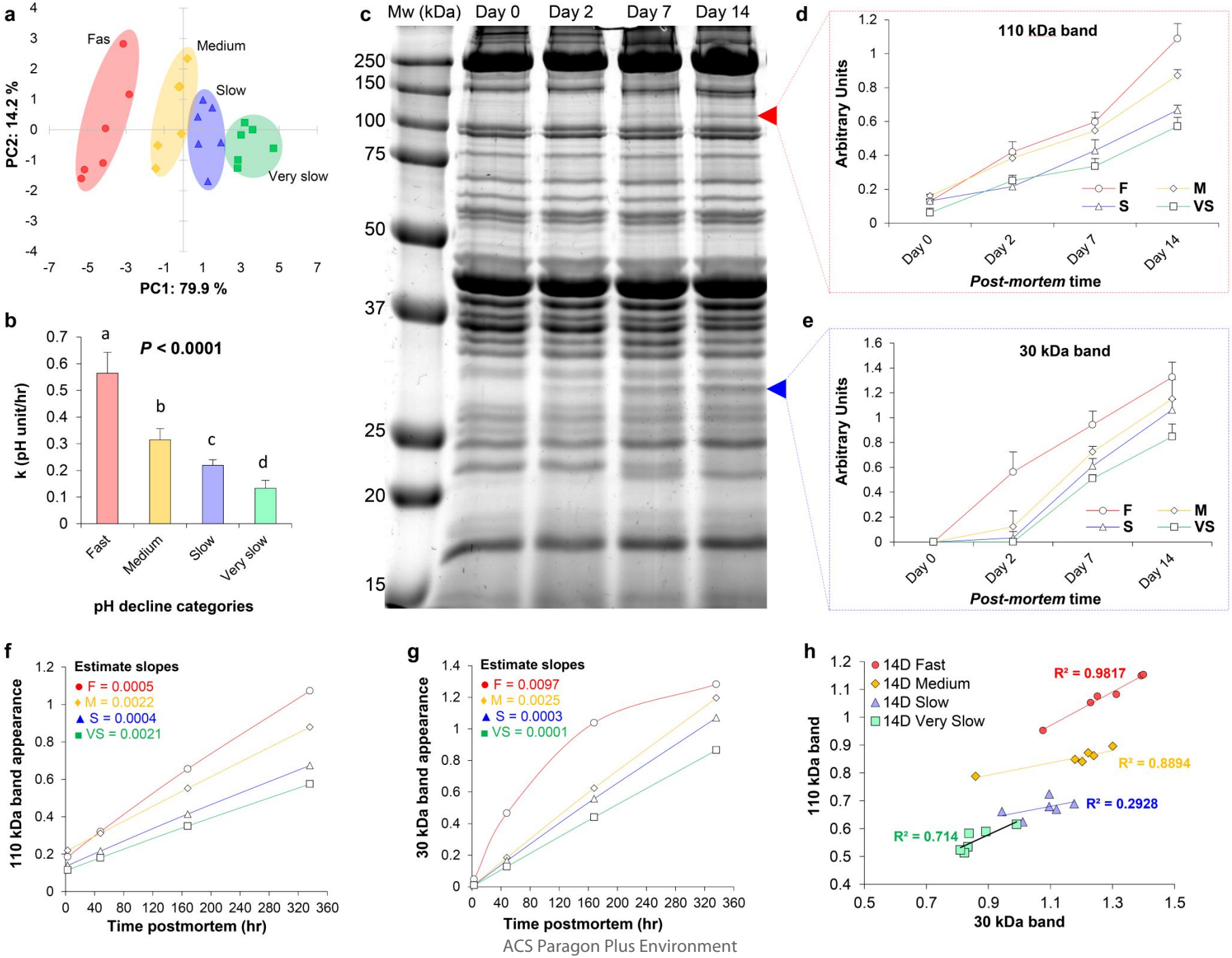
a
Fas
Medium
Slow
Very slow
PC2: 14.2 %
PC1: 79.9 %
b
P < 0.0001
k (pH unit/hr)
Fast
Medium
Slow
Very slow
pH decline categories
c
Mw (kDa)
Day 0
Day 2
Day 7
Day 14
250
150
100
75
50
37
25
20
15
d
110 kDa band
Arbitrary Units
F
M
S
VS
Post-mortem time
e
30 kDa band
f
Estimate slopes
F = 0.0005
M = 0.0022
S = 0.0004
VS = 0.0021
110 kDa band appearance
Time postmortem (hr)
g
Estimate slopes
F = 0.0097
M = 0.0025
S = 0.0003
VS = 0.0001
30 kDa band appearance
Time postmortem (hr)
h
14D Fast
14D Medium
14D Slow
14D Very Slow
R² = 0.9817
R² = 0.8894
R² = 0.2928
R² = 0.714
110 kDa band
30 kDa band

Figure 1.

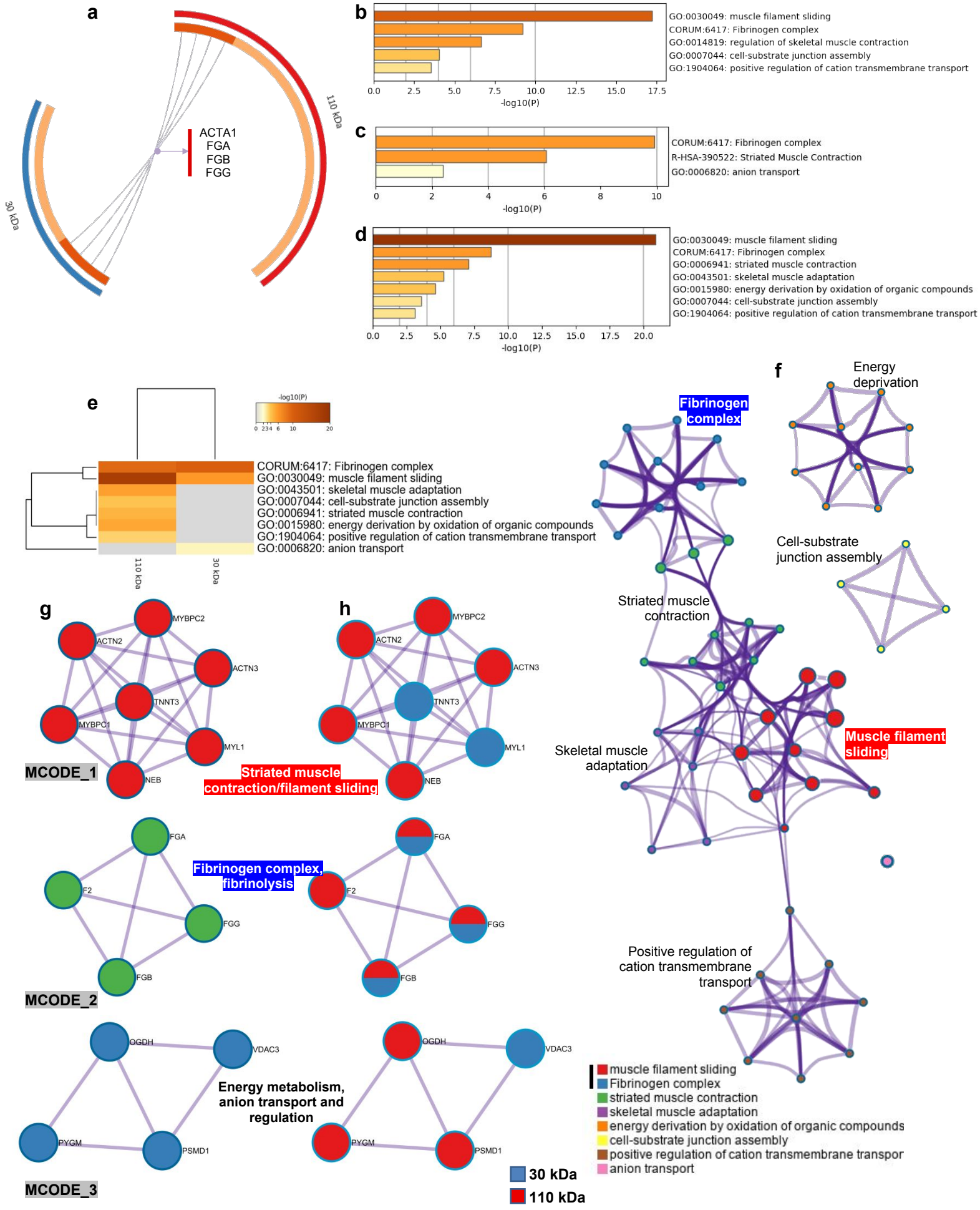
a
ACTA1
FGA
FGB
FGG
110 kDa
30 kDa
b
GO:0030049: muscle filament sliding
CORUM:6417: Fibrinogen complex
GO:0014819: regulation of skeletal muscle contraction
GO:0007044: cell-substrate junction assembly
GO:1904064: positive regulation of cation transmembrane transport
-log10(P)
c
CORUM:6417: Fibrinogen complex
R-HSA-390522: Striated Muscle Contraction
GO:0006820: anion transport
-log10(P)
d
GO:0030049: muscle filament sliding
CORUM:6417: Fibrinogen complex
GO:0006941: striated muscle contraction
GO:0043501: skeletal muscle adaptation
GO:0015980: energy derivation by oxidation of organic compounds
GO:0007044: cell-substrate junction assembly
GO:1904064: positive regulation of cation transmembrane transport
-log10(P)
e
-log10(P)
CORUM:6417: Fibrinogen complex
GO:0030049: muscle filament sliding
GO:0043501: skeletal muscle adaptation
GO:0007044: cell-substrate junction assembly
GO:0006941: striated muscle contraction
GO:0015980: energy derivation by oxidation of organic compounds
GO:1904064: positive regulation of cation transmembrane transport
GO:0006820: anion transport
110 kDa
30 kDa
f
Energy deprivation
Fibrinogen complex
Cell-substrate junction assembly
Striated muscle contraction
Skeletal muscle adaptation
Muscle filament sliding
Positive regulation of cation transmembrane transport
g
MYBPC2
ACTN2
ACTN3
TNNT3
MYBPC1
MYL1
NEB
MCODE_1
Striated muscle contraction/filament sliding
h
MYBPC2
ACTN2
ACTN3
TNNT3
MYBPC1
MYL1
NEB
FGA
F2
FGG
FGB
Fibrinogen complex, fibrinolysis
MCODE_2
OGDH
VDAC3
PYGM
PSMD1
Energy metabolism, anion transport and regulation
MCODE_3
muscle filament sliding
Fibrinogen complex
striated muscle contraction
skeletal muscle adaptation
energy derivation by oxidation of organic compounds
cell-substrate junction assembly
positive regulation of cation transmembrane transpor
anion transport
30 kDa
110 kDa

Figure 2.

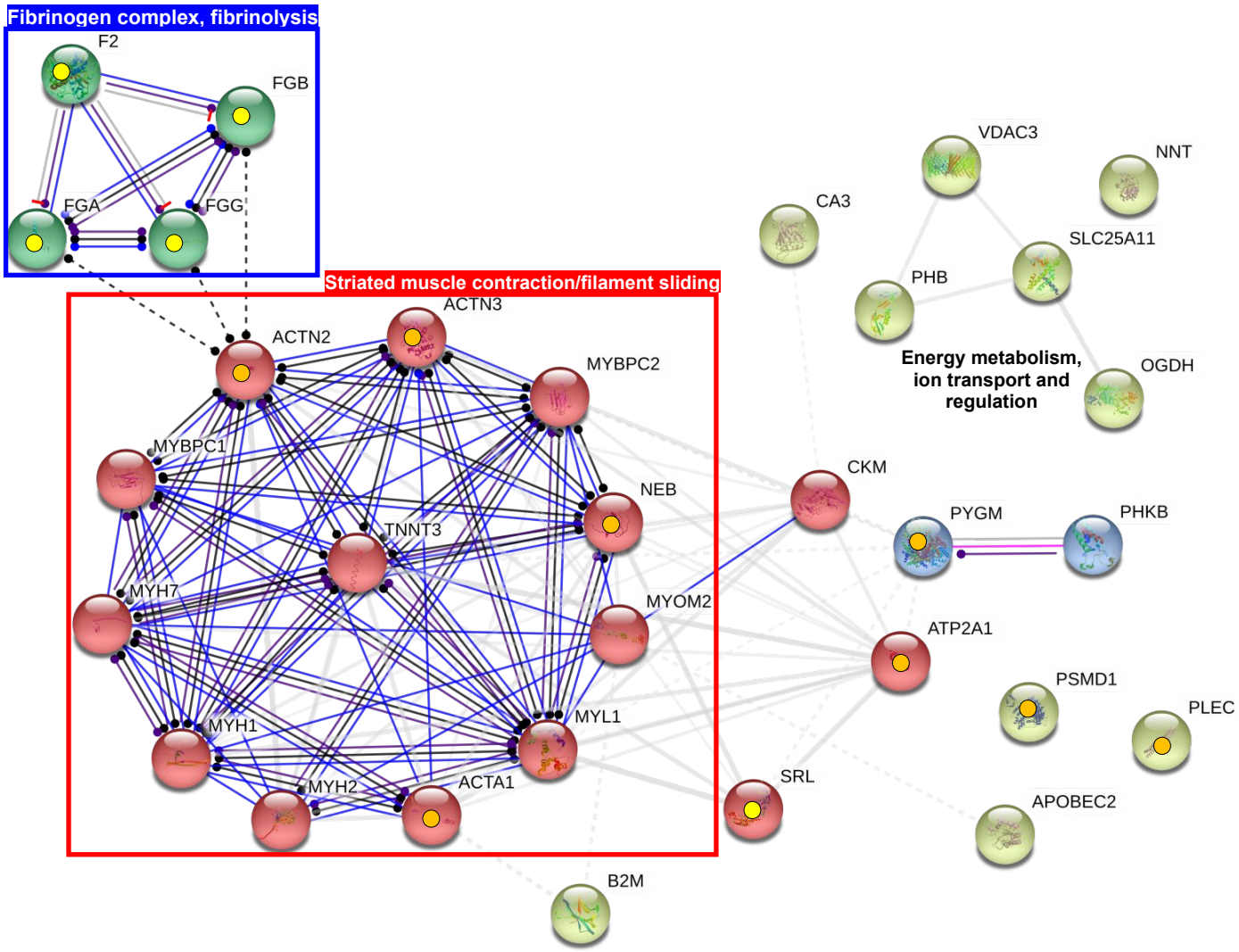
Fibrinogen complex, fibrinolysis
F2
FGB
FGA
FGG
Striated muscle contraction/filament sliding
ACTN3
ACTN2
MYBPC2
MYBPC1
NEB
TNNT3
MYH7
MYOM2
MYH1
MYL1
MYH2
ACTA1
VDAC3
NNT
CA3
SLC25A11
PHB
Energy metabolism, ion transport and regulation
OGDH
CKM
PYGM
PHKB
ATP2A1
PSMD1
PLEC
SRL
APOBEC2
B2M

Figure 3.

Table 1. LC–MS/MS (Q Exactive HF-X) identified 22 proteins from the 110 kDa proteolytic fragment band separated by 12% 1D SDS–PAGE from beef *M. longissimus thoracis et lumborum* muscle during aging.

Accession number	Gene name	Full protein name	#Peptides	Coverage, %	Secreted protein [1]	Already identified in the literature (proteomics) to be related with beef		
						Tenderness [2]	Colour [3]	pH drop
Muscle contraction and structure								
Q9BE39	MYH7	Myosin-7	21	34.26	×	✓	✓	✓
Q9BE41	MYH2	Myosin-2	44	40.98	×	✓	✓	✓
Q9BE40	MYH1	Myosin-1	52	45.15	×	✓	✓	✓
P68138	ACTA1	Actin, alpha skeletal muscle	13	44.30	✓✓	✓	✓	✓
Q3ZC55	ACTN2	Alpha-actinin-2	22	28.30	✓✓	✓	×	✓
Q0III9	ACTN3	Alpha-actinin-3	30	40.84	✓✓	✓	✓	×
A0A3Q1MC60	NEB	Nebulin	22	4.84	✓✓	✓	×	×, sheep
E1BF59	PLEC	Plectin	30	8.24	✓✓	×, pork	×	×, pork
A6QP89	MYBPC1	Myosin-binding protein C, slow-type	36	39.23	×	✓	✓	×
E1BNV1	MYBPC2	Myosin-binding protein C, fast-type	12	37.77	×	✓	×, isoform yes	×
E1BF23	MYOM2	Myomesin-2	17	30.70	×	✓	✓	✓
Catalytic and energy metabolism								
P79334	PYGM	Glycogen phosphorylase, muscle form	10	26.48	✓✓	✓	✓	✓
Q148N0	OGDH	2-oxoglutarate dehydrogenase, mitochondrial	5	4.59	×	✓	×	×
F1MJ90	PHKB	Glycogen phosphorylase kinase β-subunit	12	21.86	×	×	×	✓
P11024	NNT	NAD(P) transhydrogenase, mitochondrial	6	7.92	×	✓	×	✓
Vascular ECM glycoproteins and fibrinogen complex								
P02672	FGA	Fibrinogen alpha chain	12	32.03	✓	×, pork	×, isoform yes	×
P02676	FGB	Fibrinogen beta chain	11	44.65	✓	×, pork	✓	×
P12799	FGG	Fibrinogen gamma chain	6	33.33	✓	×, pork	×, isoform yes	×
Proteolysis								
P00735	F2	Prothrombin	4	5.28	✓	✓	×	×
A7MBA2	PSMD1	26S proteasome non-ATPase regulatory subunit 1	4	3.99	✓✓	✓	×, isoform yes	×
Calcium binding and apoptotic mitochondrial changes								
Q0VCY0	ATP2A1	Sarcoplasmic/endoplasmic reticulum calcium ATPase 1	12	15.21	✓✓	✓	×, isoform yes	✓
F1MJW7	SRL	Sarcalumenin	9	17.19	✓	✓	×	×, pork

[1] Prediction of secreted proteins was performed by the ProteINSIDE tool (http://www.proteinside.org/) identifying those potentially secreted through a signal peptide (✓) using the Signal P algorithm and by pathways that do not involve a signal peptide (✓✓) using the TargetP algorithm. If not validated, this was mentioned by a "×".

[2] The validation (✓) was mostly performed based on the integromics database on beef tenderness biomarkers from Gagaoua *et al.*[13] and also from other studies, species and muscles if not found in the corpus. If the protein isoform instead of the protein in question that is identified, this was accordingly specified.

[3] The validation was mostly performed based on the integromics database on beef colour biomarkers from Gagaoua *et al.*[4] and also from other studies, species and muscles if not found in the corpus.

Table 2. LC–MS/MS (Q Exactive HF-X) identified 13 proteins from the 30 kDa proteolytic fragment band separated by 12% 1D SDS–PAGE from beef *M. longissimus thoracis et lumborum* muscle during aging.

Accession number	Gene name	Full protein name	#Peptides	Coverage, %	Secreted protein [1]	Already identified in the literature (proteomics) to be related with beef		
						Tenderness [2]	Colour [3]	pH drop
Muscle contraction and structure								
P68138	ACTA1 [4]	Actin, alpha skeletal muscle	13	44.30	✓✓	✓	✓	✓
Q8MKI3	TNNT3	Troponin T, fast skeletal muscle	20	42.07	×	✓	×	×, pork
A0JNJ5	MYL1	Myosin light chain 1/3, skeletal muscle isoform	17	73.96	×	✓	✓	✓
Catalytic and energy metabolism								
Q9XSC6	CKM	Creatine kinase M-type	8	46.19	×	✓	✓	✓
P22292	SLC25A11	Mitochondrial 2-oxoglutarate/malate carrier protein	4	19.75	×	✓	×	×
Vascular ECM glycoproteins and fibrinogen complex								
P02672	FGA [4]	Fibrinogen alpha chain	12	32.03	✓	×, pork	×, isoform yes	×
P02676	FGB [4]	Fibrinogen beta chain	11	44.65	✓	×, pork	✓	×
P12799	FGG [4]	Fibrinogen gamma chain	6	33.33	✓	×, pork	×, isoform yes	×
Protein-binding, calcium, ion transport and apoptosis								
P01888	B2M	Beta-2-microglobulin	6	42.07	✓	×, pork	×	×, pork
Q9MZ13	VDAC3	Voltage-dependent anion-selective channel protein 3	4	19.64	✓✓	✓	×	✓
Q3T165	PHB	Prohibitin	4	18.75	✓✓	✓	×	×, pork
Q3SZX4	CA3	Carbonic anhydrase 3	4	17.69	×	✓	✓	✓
Q3SYR3	APOBEC2	C->U-editing enzyme APOBEC-2	5	21.88	×	✓	✓	×

[1] Prediction of secreted proteins was performed by the ProteINSIDE tool (http://www.proteinside.org/) identifying those potentially secreted through a signal peptide (✓) using the Signal P algorithm and by pathways that do not involve a signal peptide (✓✓) using the TargetP algorithm. If not validated, this was mentioned by a "×".

[2] The validation (✓) was mostly performed based on the integromics database on beef tenderness biomarkers from Gagaoua *et al.*[13] and also from other studies, species and muscles if not found in the corpus. If the protein isoform instead of the protein in question that is identified, this was accordingly specified.

[3] The validation was mostly performed based on the integromics database on beef colour biomarkers from Gagaoua *et al.*[4] and also from other studies, species and muscles if not found in the corpus.

[4] Common proteins with the 110 kDa protein fragment band.

Table 3. Top 8 significant clusters with their representative enriched terms (one per cluster) using the total 31 proteins identified from the two proteolytic bands (110 and 30 kDa).

Pattern [1]	Gene Ontology	Category	Description	Count [2]	% [3]	Log10(P) [4]	Log10(q) [5]
■■	GO:0030049	GO Biological Processes	muscle filament sliding	10	32.26	-20.87	-16.86
■■	CORUM:6417	CORUM	Fibrinogen complex	3	23.08	-9.93	-6.53
■	GO:0006941	GO Biological Processes	striated muscle contraction	6	19.35	-7.08	-3.96
■	GO:0043501	GO Biological Processes	skeletal muscle adaptation	3	13.64	-5.69	-3.2
■	GO:0015980	GO Biological Processes	energy derivation by oxidation of organic compounds	5	22.73	-5.37	-2.99
■	GO:0007044	GO Biological Processes	cell-substrate junction assembly	3	13.64	-4.02	-2.01
■	GO:1904064	GO Biological Processes	positive regulation of cation transmembrane transport	3	13.64	-3.54	-1.61
■	GO:0006820	GO Biological Processes	anion transport	3	23.08	-2.38	-0.64

[1] The colour code used to distinguish the protein lists among the two proteolytic bands, ■ 110 kDa and ■ 30 kDa, where the term is found statistically significant, *i.e.,* multiple colours indicate a pathway/process that is shared across the two protein lists.

[2] The number of protein names from the 33 proteins related to proteolysis of the fragments 110 and 30 kDa with membership in the given ontology term.

[3] Percentage of protein among the total list of proteins found in the given ontology term (only input genes with at least one ontology term annotation are included in the calculation).

[4] The *p*-value in log base 10.

[5] The multi-test adjusted *p*-value in log base 10. An adjusted (Benjamini–Hochberg corrected) p-value < 0.05 was considered as the threshold for statistical significance.

Table 4. Quantitative trait loci (QTL) of meat quality traits among the list of 31 identified proteins in the 110 and 30 kDa protein bands (fragments) from beef *M. longissimus thoracis et lumborum* related to beef tenderness (sensory and shear force) and meat colour lightness (*L**).

QTL linked to QTLdb [a]	Gene Name	Proteolytic band (fragment)	Full protein Name	UniProt ID	Chromosome
Tenderness score	TNNT3	30 kDa	Troponin T, fast skeletal muscle	Q8MKI4	Chr.29
	ACTN3	110 kDa	Alpha-actinin-3	Q0III9	Chr.29
	PYGM	110 kDa	Glycogen phosphorylase, muscle form	P79334	Chr.29
Shear force	PYGM	110 kDa	Glycogen phosphorylase, muscle form	P79334	Chr.29
	MYBPC1	110 kDa	Myosin binding protein C, slow type	E1BNV1	Chr.5
	F2	110 kDa	Prothrombin	P00735	Chr.15
	CA3	30 kDa	Carbonic anhydrase 3	Q3SZX4	Chr.14
	VDAC3	30 kDa	Voltage-dependent anion-selective channel protein 3	Q9MZ13	Chr.27
Meat color *L**	CKM	30 kDa	Creatine kinase M-type	Q9XSC6	Chr.18
	PHB	30 kDa	Prohibitin	Q3T165	Chr.19

[a] ProteQTL tool included in ProteINSIDE tool (http://www.proteinside.org/) interrogates a public library of published QTL in the Animal QTL Database (https://www.animalgenome.org/QTLdb/) that contains cattle QTL and association data curated from published scientific articles.

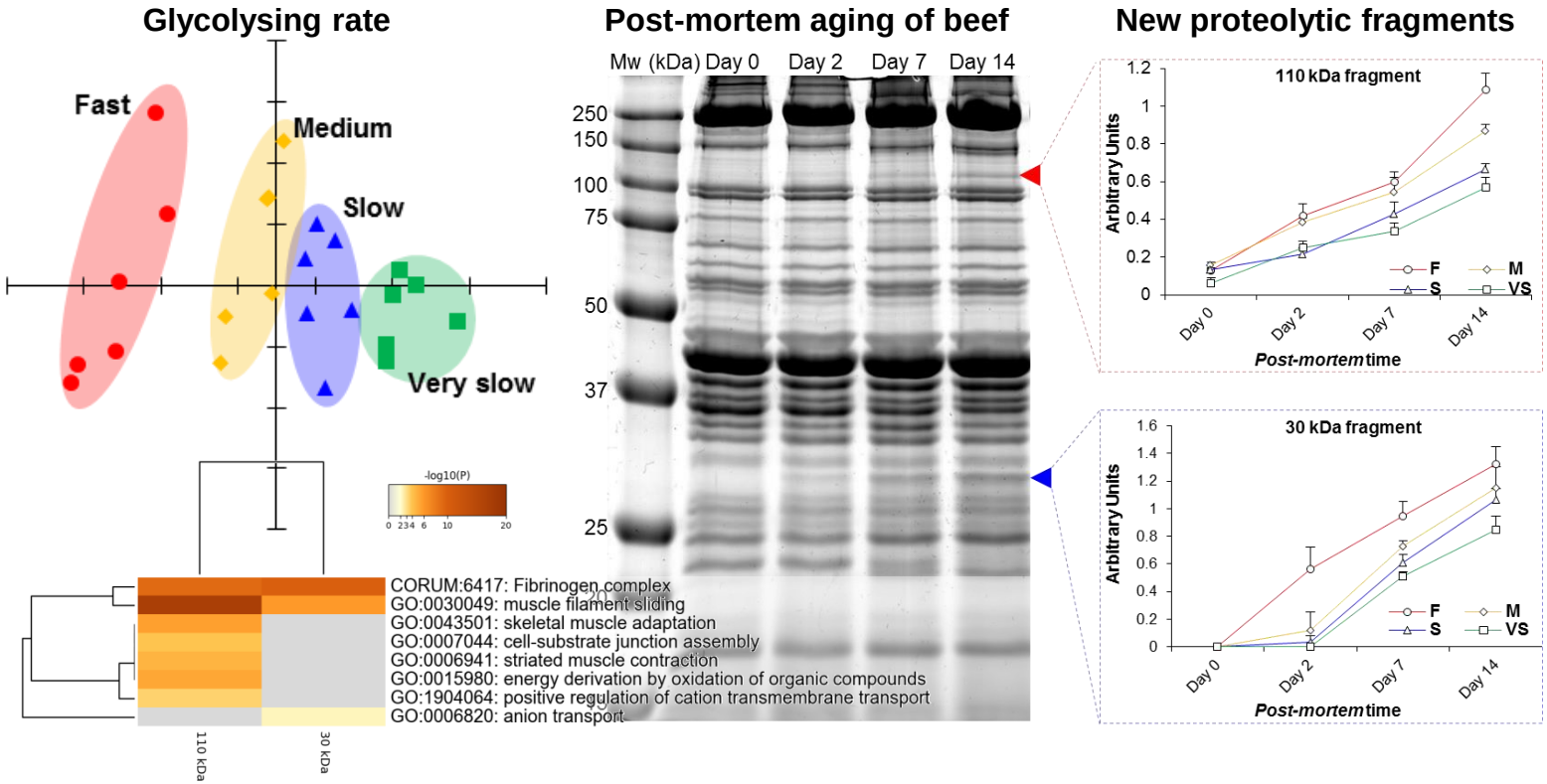
Glycolysing rate
Fast
Medium
Slow
Very slow
-log10(P)
0 2 3 4 6 10 20
CORUM:6417: Fibrinogen complex
GO:0030049: muscle filament sliding
GO:0043501: skeletal muscle adaptation
GO:0007044: cell-substrate junction assembly
GO:0006941: striated muscle contraction
GO:0015980: energy derivation by oxidation of organic compounds
GO:1904064: positive regulation of cation transmembrane transport
GO:0006820: anion transport
110 kDa
30 kDa
Post-mortem aging of beef
Mw (kDa) Day 0 Day 2 Day 7 Day 14
250
150
100
75
50
37
25
New proteolytic fragments
110 kDa fragment
Arbitrary Units
1.2
1
0.8
0.6
0.4
0.2
0
F
M
S
VS
Day 0
Day 2
Day 7
Day 14
Post-mortem time
30 kDa fragment
Arbitrary Units
1.6
1.4
1.2
1
0.8
0.6
0.4
0.2
0
F
M
S
VS
Day 0
Day 2
Day 7
Day 14
Post-mortem time